IEEE Photonics Journal
An IEEE Photonics Society Publication

Open Access

# Point Spread Function Measurement Based on Single-Pixel Imaging

Volume 10, Number 6, December 2018

Hongzhi Jiang
Yangchenxu Liu
Xudong Li
Huijie Zhao
Feng Liu

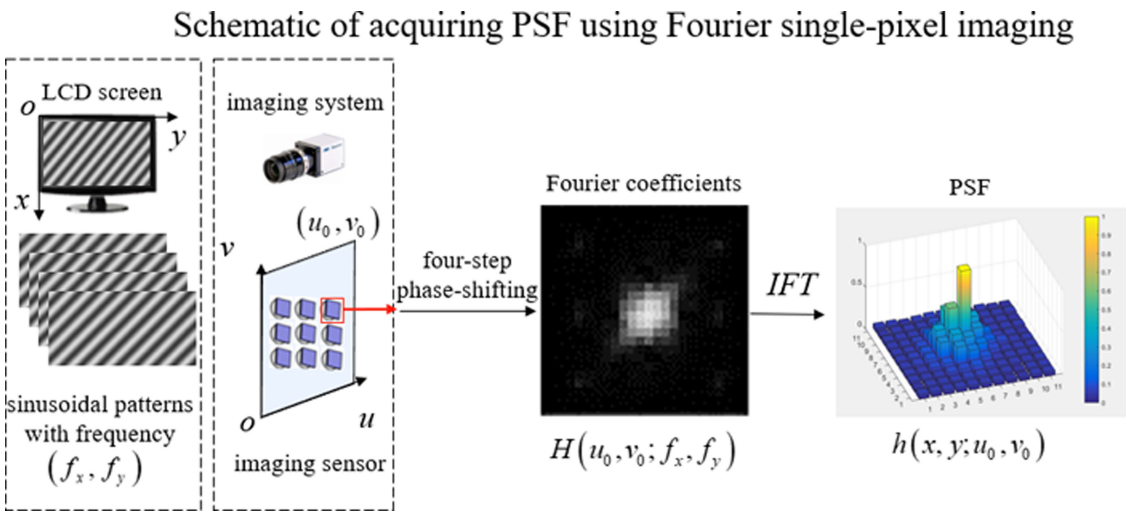


DOI: 10.1109/JPHOT.2018.2873748
1943-0655 © 2018 IEEE

IEEE photonics SOCIETY

IEEE

# Point Spread Function Measurement Based on Single-Pixel Imaging

**Hongzhi Jiang**,[1,2] **Yangchenxu Liu**,[1] **Xudong Li**,[1] **Huijie Zhao**,[1] **and Feng Liu**[2]

[1]Key Laboratory of Precision Opto-Mechatronics Technology, School of Instrumentation and Optoelectronic Engineering, Beihang University, Ministry of Education, Beijing 100191, China
[2]Key Laboratory of Micro Opto-electro Mechanical System Technology, Tianjin University, Ministry of Education, Tianjin, 300072, China

*DOI:10.1109/JPHOT.2018.2873748*


Manuscript received August 2, 2018; revised September 19, 2018; accepted September 27, 2018. Date of publication October 15, 2018; date of current version November 2, 2018. This work was supported in part by the National Natural Science Foundation of China under Grant 61475013, Grant 61735003, and Grant 61378066, in part by the Program for Changjiang Scholars and Innovative Research Team in University under Grant IRT_16R02, and in part by the open project of Key Laboratory of Micro Opto-electro Mechanical System Technology, Tianjin University, Ministry of Education. Corresponding authors: X. Li and H. Zhao (e-mail: xdli@buaa.edu.cn; hjzhao@buaa.edu.cn).

**Abstract:** Point spread function (PSF) plays an important role in evaluating the quality of optical systems and imaging restoration. Conventional methods, which use a point-like source, acquire the PSF from the perspective of object points and suffer the problem of generating multiple point sources with sufficient intensity. Thus, in this study, we proposed a novel method to measure the PSF from the perspective of camera pixels. We considered spatially varying PSF as the light transport coefficients between the object and image points. By applying single-pixel imaging technology to every pixel of the image plane of a camera, PSF is extracted from the obtained light transport coefficients. Experiments also verified that the proposed method could achieve better signal-to-noise ratio PSF measurement than the conventional method and acquire an accurate blur model of the camera lens.

**Index Terms:** Point spread function, imaging formation theory, computational imaging.

## 1. Introduction

Point spread function (PSF), also known as the impulse response of an imaging system, can cause inevitable image degradation during exposure. Although extrinsic blur, such as camera motion, can be prevented by improving the acquisition conditions, the intrinsic properties of the optical system, such as lens aberration and diffraction, also have a profound effect on image quality. Given the prior condition of image restoration, accurate measurement of the PSF can be extremely significant [1].

Several techniques have been produced to obtain PSF. We divide the PSF acquisition methods into three categories based on their input images as follows: blind PSF estimation using natural scene images [2]–[4], non-blind PSF estimation using calibrated patterns [4]–[7], and PSF direct measurement using a point-like source [8]–[11].

Blind PSF estimation methods estimate PSF using a blurred scene image and the corresponding underlying sharp image. This method often utilizes the edge feature of an input scene to restore sharp images and obtains PSF through optimization. Joshi *et al.* [4] directly assumed that the detected blurred edge was a step edge before blurring and estimated PSF using the pair of predicted

sharp image and blurred image. Sun *et al.* [2] proposed another edge-based approach that could restore high-quality sharp images to estimate PSF using patch priors on the edges of the latent sharp image. Blind PSF estimation methods often presume a spatial invariant PSF in the sub-areas over the entire image and are thus not suitable for acquiring the spatial variant PSF.

Non-blind PSF estimation method uses calibration patterns as the input image to estimate PSF [4]–[7]. After aligning the known grid calibration pattern to the blurred image, PSF is obtained through optimization. Joshi *et al.* [4] employed an arc-shaped checkerboard-like pattern and estimated PSF by using a Bayesian framework with a maximum a posteriori technique. Kee *et al.* [6] used a checkerboard test chart with circles in each block and estimated PSF by solving a least squares minimization problem. Brauers *et al.* [7] used a random noise target to estimate PSF. Non-blind PSF estimation techniques usually assume a spatial invariant PSF as well and are thus not suitable for spatial variable PSF image systems.

PSF direct measurement methods often acquire PSF using a point-like source with specific optical instruments [8]–[11]. Such methods can overcome the weakness for measuring the spatial variant PSF. Navas-Moya *et al.* [11] used a liquid crystal display (LCD) screen in generating a dot pattern to measure PSFs in different camera areas. However, this method suffered camera noise and had to use a large camera acquisition time with corresponding noise elimination method. Lehr *et al.* [9] also indicated that directly using a general point source, such as an isolated gold microbead could not achieve sufficient signal-to-noise ratio (SNR) and had to resort to the edge-based method to measure PSF. Du *et al.* [8] proposed a method adopting a collimated He–Ne laser as a point source placed at infinity for PSF measurement with high SNR. Jemec *et al.* [10] achieved a sub-pixel PSF measurement using a virtual point-like source. Although these laser-beam based methods can achieve PSF measurement with high SNR, they have difficulty in generating multiple point sources to measure the spatial variant PSF.

Therefore, the low SNR problem using a general point source and the difficulty of generating multiple point sources using laser-beam to measure the spatial variant PSF create a bottleneck in the measurement of spatial variant PSF. The development of single-pixel imaging (SPI) technology motivates us to propose a new method for PSF measurement. SPI projects known illuminated patterns onto an object and collects the intensity of the reflected light using a single-pixel detector [12], [14]. The image is then reconstructed using the collected modulated signal. Moreover, SPI that uses patterns from complete orthogonal bases [13]–[16], such as the Fourier SPI (FSI) method, can capture the desired scene indirectly and reconstruct the image with high SNR. The characteristic of high SNR imaging of SPI and its capability to obtain an image from a pixel [14], [17] inspires us to apply it for the measurement of spatial variant PSF of camera lens.

In this study, we propose a measurement method for spatial variant PSF based on SPI technology. The proposed method models the PSF as the light transport coefficients between the object and image points. By considering each pixel of the camera as a single-pixel detector, we can conduct SPI to the camera pixels and acquire the light transport coefficients between the object and image points, that is, the PSF. Our method is an SPI-based technology; thus, we can achieve higher SNR measurement than the traditional PSF measurement methods using the same camera exposure time. Furthermore, for each camera pixel, our method can calculate the image of the object light collected by the pixel, which can be regarded as the ground truth of a super-resolved blur kernel.

## 2. Principles

Different from the conventional methods that uses point-like sources to measure the spatially varying PSF, the proposed method introduces SPI technology to acquire the PSF. The main idea of our method is to consider spatially varying PSF as the light transport coefficients between the object and image points. And the coefficients can be obtained from both the perspective of object points and the perspective of image pixels.

As shown in Fig. 1(a), if the optical system is affected by defocus and lens aberration, then the light emitted from one object point will emerge in multiple camera pixels. Conventional PSF measurement methods are based on this view and measure PSF using a point-like source. Meanwhile, the light

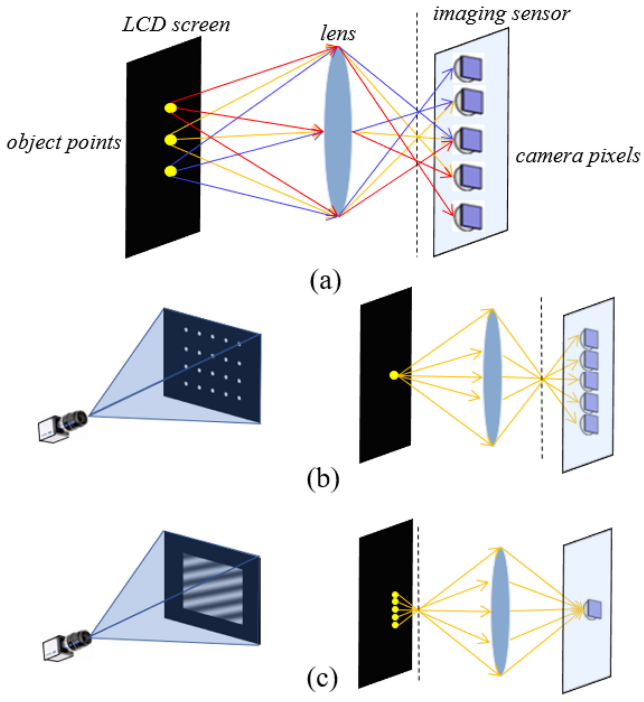


Fig. 1. Schematic of the PSF in the optical system. (a) Effect of the PSF in the optical system. (b) Conventional PSF measurement method from the perspective of object points. (c) Proposed PSF measurement method from the perspective of image pixels.

collected by one pixel in the imaging sensor can be emitted from multiple object points. This motivates us to measure the PSF from the perspective of camera pixels.

By applying SPI to a camera pixel, we can obtain the light transport coefficients from the object points to the camera pixel. Moreover, all light transport coefficients between the object and image points are acquired by applying SPI to all the camera pixels, that is, the spatial variant PSF. SPI-based PSF measurement method not only provides a more direct way to represents how the light of objects contributes to the response of the camera pixels, but also brings the characteristic of high SNR imaging of SPI into the measurement of PSF.

The differences between the proposed method and the traditional PSF measurement method are shown in Figs. 1(b) and 1(c). As shown in Fig. 1(b), the traditional PSF measurement method acquires the PSF using point sources and obtains the light transport coefficients from a point source to the pixel arrays. In Fig. 1(c), the proposed method obtains the PSF using SPI and acquires the light transport coefficients from one image pixel to the object points. Both methods can acquire the spatially varying PSF once all the light transport coefficients between the object and image points are acquired.

### 2.1 Formulating the Imaging Formation Model

We analyze the image formation process for a single camera pixel using SPI technology based on complete orthogonal bases and provide an analytical derivation of SPI-based PSF measurement.

In the general case of an optical system with spatial variant PSF, the image formation process can be modeled as

$$I(u, v) = \iint_{\Omega} O(x, y) \cdot h(x, y; u, v) dx dy, \tag{1}$$

where $\Omega$ represents the observed area of the input scene; $I$ is the acquired image; $(u, v)$ denotes the 2D Cartesian coordinates on the image plane; $O$ represents the input scene; $(x, y)$ denotes the

2D Cartesian coordinates on the object plane; h($x$, $y$; $u$, $v$) denotes the spatially varying PSF of the optical system, which also represents the light transport coefficients between the object point ($x$, $y$) and the image point ($u$, $v$).

If we regard the camera pixel ($u$, $v$) as a single-pixel detector, then Eq. (1) will represent the response of a single-pixel detector in a single measurement. Moreover, if we can modulate the input scene $O(x, y)$ and use it as an image forward transform kernel, then one coefficient in the transform domain of $h(x, y; u, v)$ will be obtained, which can be written as

$$H(m, n; u, v) = \iint_{\Omega'} r(x, y, m, n; u, v) \cdot h(x, y; u, v) dx dy, \tag{2}$$

where $\Omega'$ represents the modulated area of the input scene, $H(m, n; u, v)$ denotes the coefficients of $h(x, y; u, v)$ in the transform domain, and $r(x, y, m, n; u, v)$ represents the forward transform kernel produced by the input scene $O(x, y)$. Applying the inverse transform to $H(m, n; u, v)$ yields

$$h(x, y; u, v) = \iint_{\Phi} s(x, y, m, n; u, v) \cdot H(m, n; u, v) dm dn, \tag{3}$$

where $\Phi$ represents the transform domain area corresponding to the input scene, and $s(x, y, m, n; u, v)$ denotes the inverse transform kernel corresponding to $r(x, y, m, n; u, v)$. Equations (2) and (3) indicate that the spatially varying PSF $h(x, y; u, v)$ can be acquired by applying SPI to all the camera pixels. SPI, which uses the patterns of standard orthonormal bases, is proposed to acquired high-quality 2D images and high SNR [17]; thus, we adopt the FSI method to achieve an accurate PSF measurement. The details of the method are introduced in the next sub-section. Here, we are considering the FSI method only. Of course, other kind of SPI method can also be used to measure the PSF.

### 2.2 FSI-Based PSF Measurement

We formulate the FSI-based measurement method for spatially varying PSF. The FSI method acquires the Fourier coefficients of a scene by illuminating the detected object with phase-shifting sinusoidal-structured light patterns using a detector without spatial resolution. The reflectivity of the captured object is then obtained by applying inverse Fourier transform (IFT) to the acquired Fourier spectrum of the object [14].

In our method, we use an LCD screen to display the sinusoidal-structured light patterns used in FSI [14] as the modulation of the input scene. An industrial camera is employed to collect the Fourier coefficients. Every camera pixel can be regarded as an SPI detector; thus, we can obtain an image that represents the spatially varying PSF $h(x, y; u, v)$ of the camera pixel ($u$, $v$) by applying IFT to a camera pixel. The image also represents the light emitted from the LCD screen point ($x$, $y$), which the camera pixel ($u$, $v$) can collect. We show the imaging system setup of the proposed FSI-based PSF measurement in Fig. 2.

To measure the PSF, the illumination pattern $P\varphi$ from FSI [14] is displayed on the LCD screen [Fig. 3(a)], which can be expressed as follows:

$$P_{\varphi}(x, y; f_x, f_y) = a + b \cdot \cos\left(2\pi f_x x + 2\pi f_y y + \varphi\right), \tag{4}$$

where ($x$, $y$) denotes the 2D Cartesian coordinates on the LCD plane, ($f_x$, $f_y$) represents the spatial frequency of the sinusoid pattern, $\varphi$ is the pattern initial phase, a is the average image intensity, and b is the amplitude of the sinusoid pattern. A camera is used to collect the light emitted by the LCD screen. Thus, the response $R\varphi$ of the camera is obtained as follows:

$$R_{\varphi}(u, v; f_x, f_y) = \iint_{\Omega} P_{\varphi}(x, y; f_x, f_y) \cdot h(x, y; u, v) dx dy + R_n, \tag{5}$$

where $\Omega$ represents the illumination area generated by the screen, ($u$, $v$) denotes the 2D Cartesian coordinates on the camera pixel plane, $h(x, y; u, v)$ is the spatially varying PSF for the optical system, and $R_n$ is the response of the camera pixel to environmental light. Then, the four-step

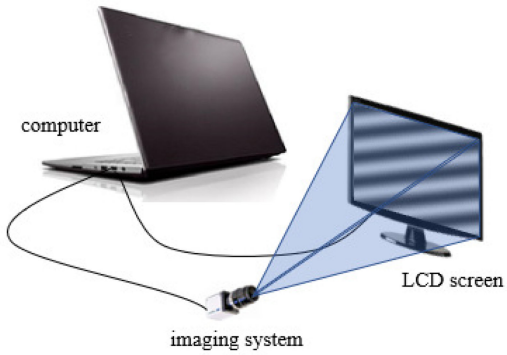


Fig. 2. Imaging system setup of the FSI-based PSF measurement. The LCD screen displays the sinusoidal-structured light patterns. The camera captures the pattern on the screen. PSF is then calculated using the obtained data.

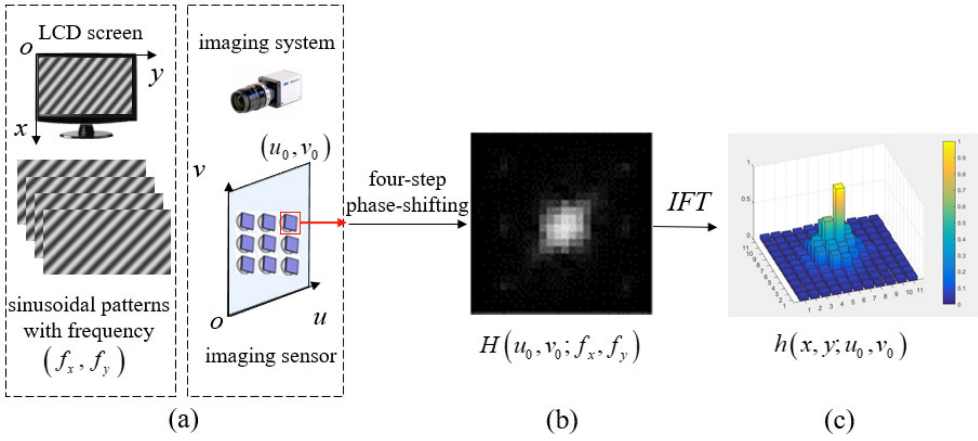


Fig. 3. Schematic of acquiring PSF using FSI. (a) The camera captures the sinusoidal patterns on the LCD screen as the modulate input scene. (b) The four-step phase-shifting method is applied to the captured signal of pixel ($u_0$, $v_0$) to obtain the Fourier coefficients $H(u_0, v_0; f_x, f_y)$. (c) IFT is performed to $H(u_0, v_0; f_x, f_y)$ to calculate the collected image of the object light by pixel ($u_0$, $v_0$).

phase-shifting method is used to acquire the Fourier coefficients by modulating the illumination pattern $P_\varphi$. For a specific spatial frequency ($f_x$, $f_y$), we can change the phase $\varphi$ (0, $\pi/2$, $\pi$, $3/2\pi$) of the pattern to obtain one Fourier coefficient $H(u, v; f_x, f_y)$ that corresponds to the PSF $h(x, y; u, v)$ in the Fourier domain, which yields

$$\begin{aligned} H(u, v; f_x, f_y) &= \frac{1}{2b} \cdot \{[R_0(u, v; f_x, f_y) - R_\pi(u, v; f_x, f_y)] \\ &\quad + j \cdot [R_{\pi/2}(u, v; f_x, f_y) - R_{3\pi/2}(u, v; f_x, f_y)]\} \\ &= \iint_\Omega h(x, y; u, v) \cdot \exp[-j2\pi(f_x x + f_y y)] dx dy. \end{aligned} \tag{6}$$

The factor $\exp[-j2\pi(f_x x + f_y y)]$ is the 2D Fourier transform kernel. Equation (6) indicates that the Fourier coefficients $H(u, v; f_x, f_y)$ [Fig. 3(b)] corresponding to the PSF $h(x, y; u, v)$ can be obtained by applying the four-step phase-shifting method to the obtained camera response $R\varphi$. In the meantime, the differential measurement in Eq. (6) can efficiently remove the response of the environmental light and the direct current (DC) component.

M $\times$ N Fourier coefficients are required to obtain an M $\times$ N image of PSF $h(x, y; u, v)$, which indicates the light transport coefficients from M $\times$ N pixels of the LCD plane to the camera pixel

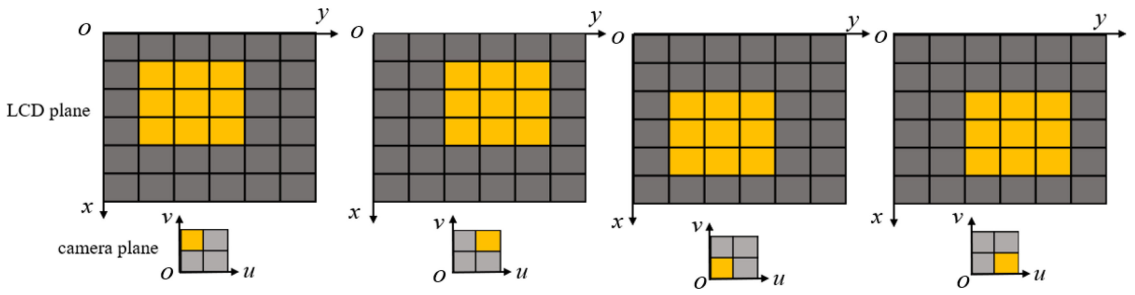


Fig. 4. Schematic of the blur kernel from Eq. (7). For each camera pixel ($u$, $v$), Eq. (7) can calculate an image that can be regarded as the blur kernel from the high-resolution LCD plane to the low-resolution camera plane.

($u$, $v$). Thus, M $\times$ N $\times$ 4 images of the sinusoid patterns should be acquired. As the Fourier spectrum is conjugate symmetric for the natural signal, only half of the images should be acquired. By conducting IFT to the acquired Fourier spectrum, $h(x, y; u, v)$ can be obtained [Fig. 3(c)], which can be expressed as follows:

$$h(x, y; u, v) = IFT(H(u, v; f_x, f_y)). \tag{7}$$

The obtained result merely corresponds to one pixel on the image plane. To measure the complete spatially varying PSF $h(x, y; u, v)$, the proposed method should be conducted to all the pixels of the camera. The calculation for all the camera pixels can be performed in parallel because the camera pixels collect the Fourier coefficients simultaneously. The entire spatially varying PSF $h(x, y; u, v)$ can be acquired by combining all the calculation results.

The schematic of acquiring $h(x, y; u_0, v_0)$ for one camera pixel $(u_0, v_0)$ using FSI is shown in Fig. 3. The camera pixels capture the sinusoidal patterns on the LCD screen. The Fourier spectrum $H(u_0, v_0; f_x, f_y)$ corresponding to camera pixel $(u_0, v_0)$ can be acquired by applying the four-step phase-shifting method to the captured signal. The light transport coefficients from the object points to the camera pixel $(u_0, v_0)$ can be obtained by applying IFT to $H(u_0, v_0; f_x, f_y)$.

Furthermore, the result from Eq. (7) can be regarded as the ground truth of the blur kernel from the high-resolution image displayed on the LCD screen to the low-resolution image captured by the camera. As shown in Fig. 4, the pixel on the low-resolution camera plane captures the light emitted from multiple pixels on the high-resolution LCD plane. The image that Eq. (7) acquires represents the true weights of the object points ($x$, $y$), which contribute to the response of the low-resolution camera pixel $(u_0, v_0)$. The image also represents the spatial variant PSF result $h(x, y; u_0, v_0)$ from the perspective of the camera pixel $(u_0, v_0)$.

### 2.3 Comparing the PSF Measurement Result

The conventional PSF measurement methods based on a point-like source merely acquire the PSF from the perspective of object point. Each measurement result obtains PSF $h(x_i, y_i; u, v)$ that corresponds to one point $(x_i, y_i)$ on the object plane. The proposed method acquires the PSF from the perspective of camera pixels. Each calculation obtains PSF $h(x, y; u_i, v_i)$ that corresponds to one pixel $(u_i, v_i)$ on the image plane.

To compare the result of the conventional method with that of the proposed method, the following process was conducted:

*Step 1:* Acquire the PSF based on conventional point-like source method. Record the point source coordinates $(x_0, y_0)$ and the PSF $h(x_0, y_0; u, v)$ distribution image. The process is shown in Fig. 5(a).

*Step 2:* Apply SPI to the camera pixel $(u_0, v_0)$ and acquire $h(x, y; u_0, v_0)$. The process is shown in Fig. 5(b).

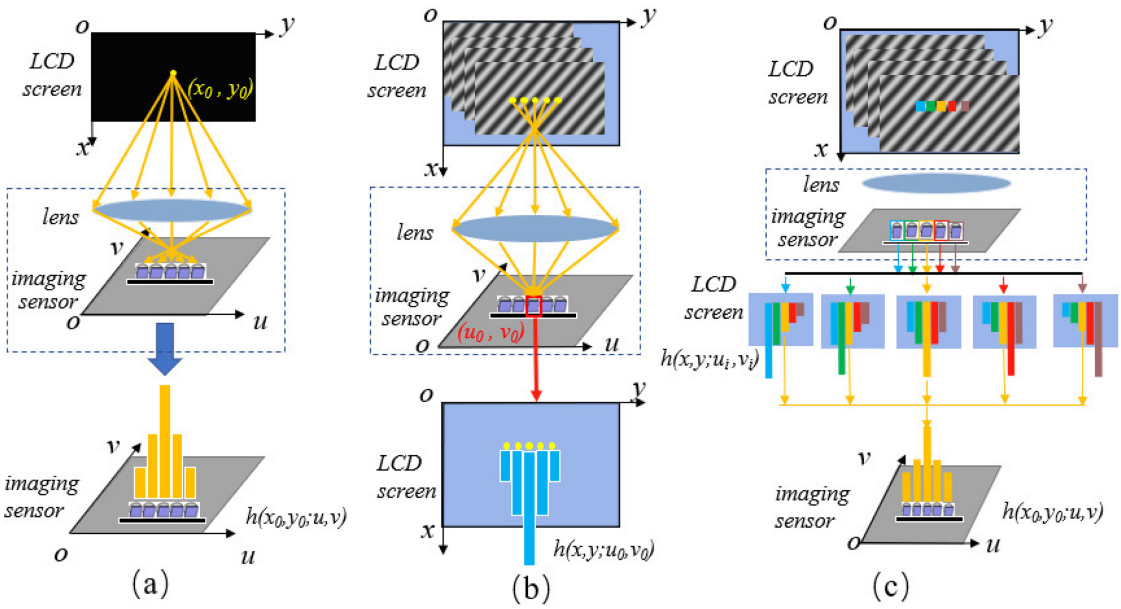


Fig. 5. Schematic of comparing the PSF result of the conventional method to that of the proposed method. (a) Schematic of acquiring $h(x_0, y_0; u, v)$ using the conventional method. (b) Schematic of acquiring $h(x, y; u_0, v_0)$ using the proposed method. (c) Process of acquiring $h(x_0, y_0; u, v)$ by the proposed method.

*Step 3:* Conduct the proposed method to all the pixels of the camera and obtain the PSF $h(x, y; u_i, v_i)$ of all the camera pixels. Thus, the spatially varying PSF $h(x, y; u, v)$ is obtained. For each SPI result $h(x, y; u_i, v_i)$, extract the value of $h(x_0, y_0; u_i, v_i)$. By recombining all the $h(x_0, y_0; u_i, v_i)$ from all the pixels $(u_i, v_i)$, the same PSF $h(x_0, y_0; u, v)$ to the result of Step 1 is obtained. Figure 5(c) shows the schematic of acquiring the PSF $h(x_0, y_0; u, v)$ using our method.

### 2.4 The Improvement of the SNR

The PSF measurement process is affected by the noise of the imaging sensor. In traditional PSF measurement method, the image of PSF is detected by the imaging sensor. The noise is directly added to the corresponding pixel value and thus causes the decrease of SNR. In proposed PSF measurement method, as shown in Eq. (5) and (6), the Fourier coefficients of the PSF image is obtained. The noise of the sensor is added to the Fourier coefficients. Furthermore, PSF is reconstructed by applying IFT to the obtained Fourier spectrum [Eq. (7)]. The pixel value in the reconstructed image is a weighted sum of all measured coefficients in the Fourier domain. Such an averaging process allows evening out errors [15], [18] and thus improves SNR of the PSF measurement.

In conclusion, the proposed method not only acquires the spatially varying PSF $h(x, y; u, v)$, which represents the light transport coefficients between the object and image points, but also obtains an accurate blur kernel that corresponds to every camera pixel. Moreover, the proposed method can achieve a better SNR measurement than the conventional method. This result can be attributed to the adopted four-step phase-shifting method which eliminates the DC term and the averaging process of IFT which evens out the errors in measurement.

## 3. Experiments

The structure of our experiment setup is shown in Fig. 6. The system is composed of an LCD screen, a camera with a lens to be tested, and a computer that controls the LCD screen and

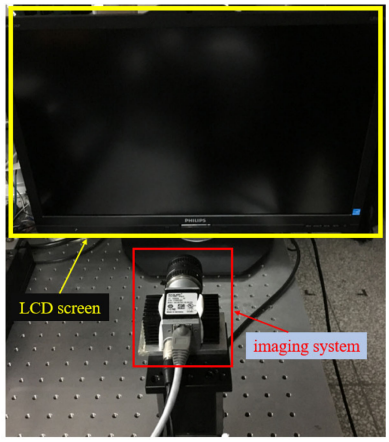


Fig. 6. Image of the experimental setup. The LCD screen is placed 0.5 m away from the camera. The sinusoidal patterns are displayed on the screen. The camera captures the patterns and transfer the data to the computer.

acquires the images. The LCD screen is a Philips 242P6VPJKEB screen with 3840 $\times$ 2160 pixels and 0.2715 mm $\times$ 0.2715 mm pixel size. A Basler acA1600-20 gm camera using a Computar lens was used to obtain the pattern images. The spatial resolution of the camera is 1600 $\times$ 1200 pixels, and the pixel size is 4.5 $\mu$m $\times$ 4.5 $\mu$m. The focal length of the lens is approximately 8 mm, and the f-number is set to 4.0. The distance between the center of the entrance pupil and the center of the LCD screen is approximately 0.5 m. The result images were acquired and processed by the computer.

We adopted the FSI approach as the SPI method for measuring the PSF due to its anti-noise and high-quality imaging characteristics. The fringe patterns with $\pi/2$ phase shifting in the same frequency were displayed on the LCD screen. The camera recorded the fringe patterns sequentially. We applied the four-step phase-shifting method to the acquired fringe patterns to obtain the Fourier coefficients for each camera pixel. We conducted the IFT to the acquired Fourier spectrum of all the camera pixels to measure the spatially varying PSF accurately.

### 3.1 Measuring the PSF of Camera Lens

The PSF measuring experiments for one area of the camera field of view were conducted to prove the accuracy of the proposed method. First, the LCD screen with 3840 $\times$ 2160 pixels was captured by the camera with 1600 $\times$ 1200 pixels to ensure that one pixel of the LCD screen could be captured in one camera pixel. Then, the fringe patterns were displayed on the 24 $\times$ 24 center area of the LCD screen. The FSI method was conducted to all the camera pixels in the corresponding fringe area on the camera plane, which occupied about 15 $\times$ 15 pixels.

Part of the FSI results are shown in Fig. 7. The FSI results of the camera pixels represent the light of the LCD pixels collected by the camera pixels. The images could also be regarded as the PSF $h(x, y; u_i, v_i)$ from the perspective of the camera pixels $(u_i, v_i)$, which can work as a blur kernel from the high-resolution LCD image to the camera pixel $(u_i, v_i)$.

We obtain the distribution of $h(8, 12; u, v)$ by applying FSI to all the camera pixels $(u_i, v_i)$ that corresponded to the fringe area and extracting the value of the FSI result $h(8, 12; u_i, v_i)$. The PSF result $h(8, 12; u, v)$ of the proposed method is shown in Fig. 8(a). We also displayed a white dot at coordinates (8, 12) on the same area of the fringe patterns on the LCD screen to acquire the traditional measurement result [11] of PSF $h(8, 12; u, v)$. The distribution result is shown in Fig. 8(b). To compare the result of the proposed method to the conventional method, we normalized the PSF results and the difference is shown in Fig. 8(d). The result in Fig. 8(d) implies that the

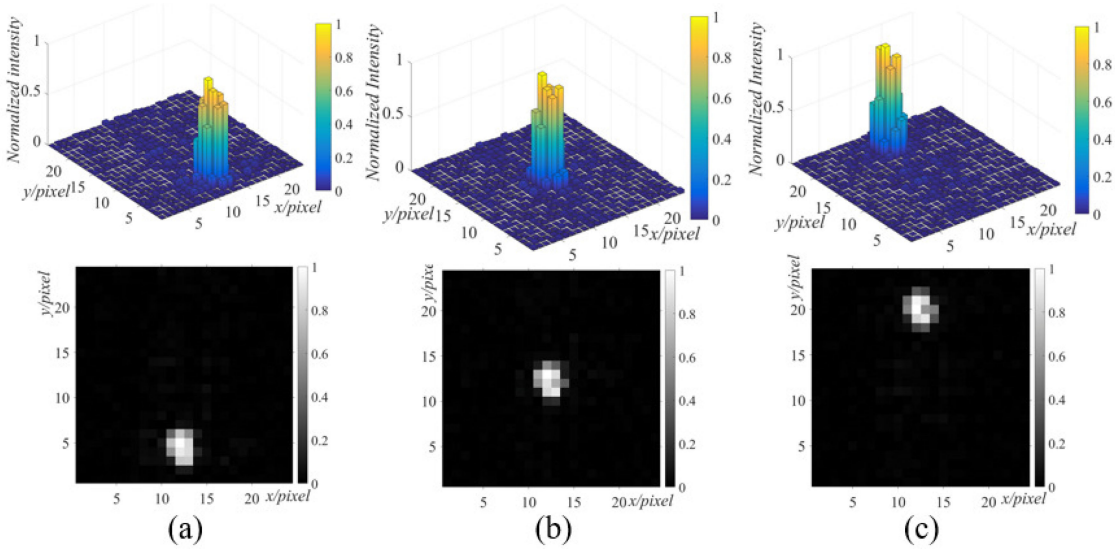


Fig. 7. Part of the FSI results of the camera pixels. The 3D bar graph and the grayscale image of FSI results of the camera pixels (7, 2), (7, 7) and (7, 12) are shown in Fig. 7(a), Fig. 7(b) and Fig. 7(c) respectively.

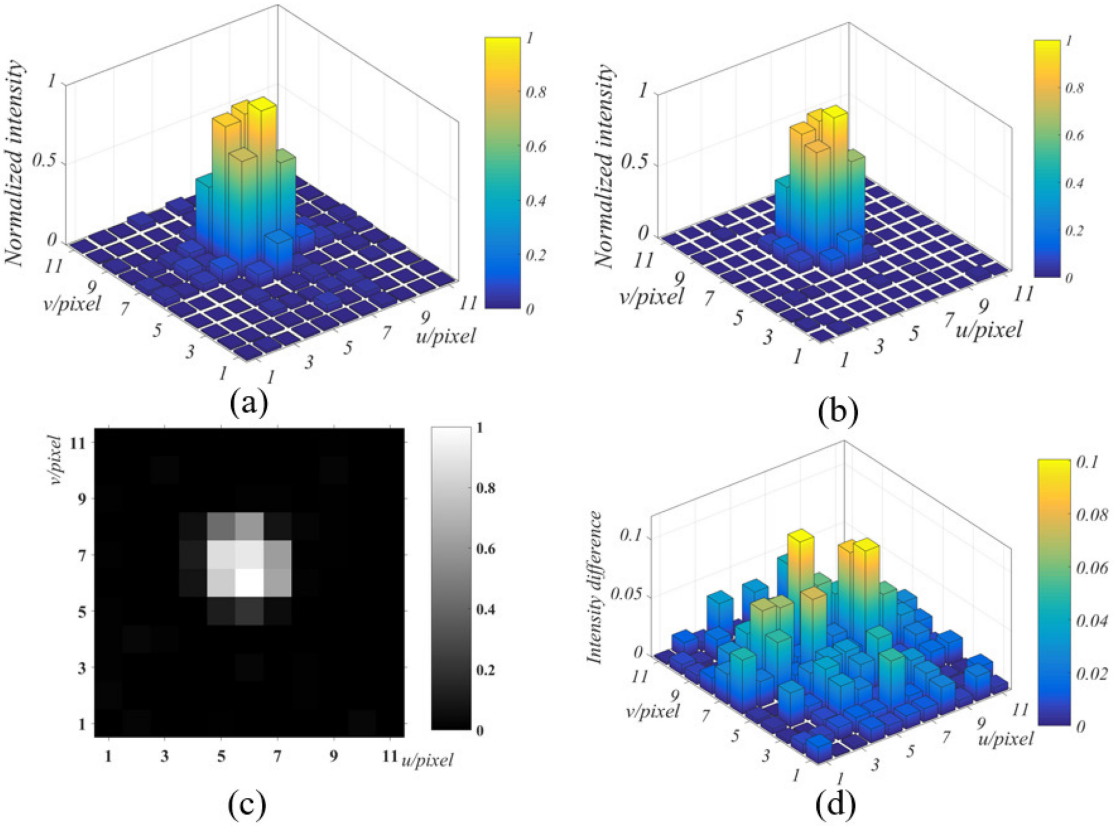


Fig. 8. PSF measurement results of the proposed method. (a) PSF result $h(8, 12; u, v)$ using the proposed method. (b) PSF result $h(8, 12; u, v)$ using the conventional method. (c) Grayscale image of $h(8, 12; u, v)$ using the proposed method. (d) Difference of the normalized PSF between the conventional and proposed methods.

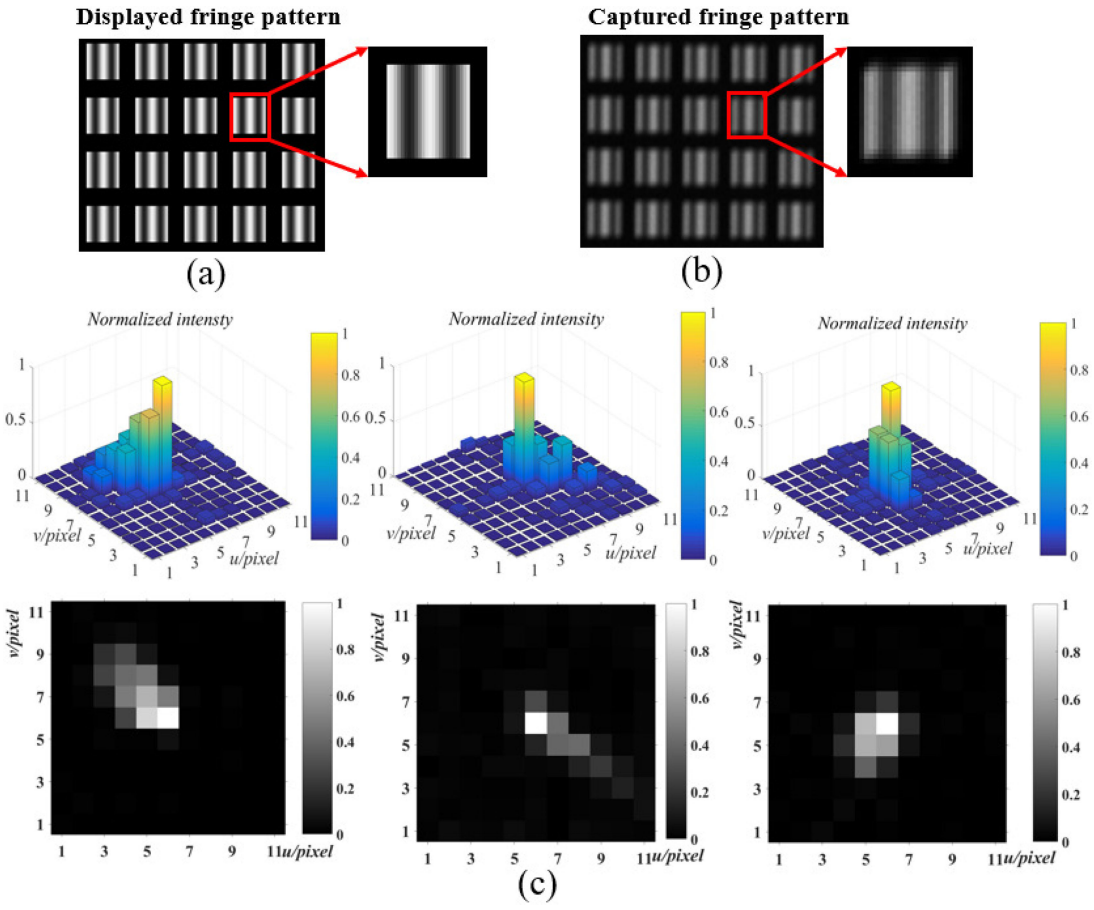


Fig. 9. One of the displayed fringe patterns used in the experiment and the obtained PSF results in different camera areas using the proposed method. (a) Part of the fringe pattern array with frequency (0, 2) used in the experiment. (b) Fringe pattern captured by the camera. (c) PSF results in different areas of the camera field of view using the proposed method.

proposed method could obtain PSF result of the camera lens like the result obtained by traditional method.

We used the proposed method based on FSI to measure the PSF in different areas in the camera field of view to verify that the PSF is spatially variable because of the wide field of view and the lens aberration. Theoretically, we can measure the spatially varying PSF $h(x, y; u, v)$ by applying FSI to all the camera pixels. In practice, to measure the PSF through the whole camera field of view, the light transport coefficients between the LCD screen pixels ($3840 \times 2160$) and the camera pixels ($1600 \times 1200$) should be acquired. According to [14], $3840 \times 2160 \times 2$ patterns of FSI are required to displayed on the LCD screen and captured by the camera, which is time-consuming. Thus, we measured the PSF efficiently by displaying $24 \times 24$ pixel-sized fringe patterns on multiple areas of the LCD screen simultaneously. Consequently, we could obtain the spatially varying PSF in the multiple fringe areas under the same time consumption as measuring the PSF in a single $24 \times 24$ fringe area. We show one of the cropped portions of the FSI-fringe patterns used in the experiment in Fig. 9(a) and the corresponding captured fringe pattern in Fig. 9(b).

For every fringe area, we applied FSI to all the camera pixels $(u_i, v_i)$ and extracted the value of $h(8, 12; u_i, v_i)$ to form the PSF distribution. The PSF results in different areas using the proposed method are shown in Fig. 9(c). The results indicate that the PSF is not only spatially variable but also radially asymmetric, especially in the edge area of the camera field of view.

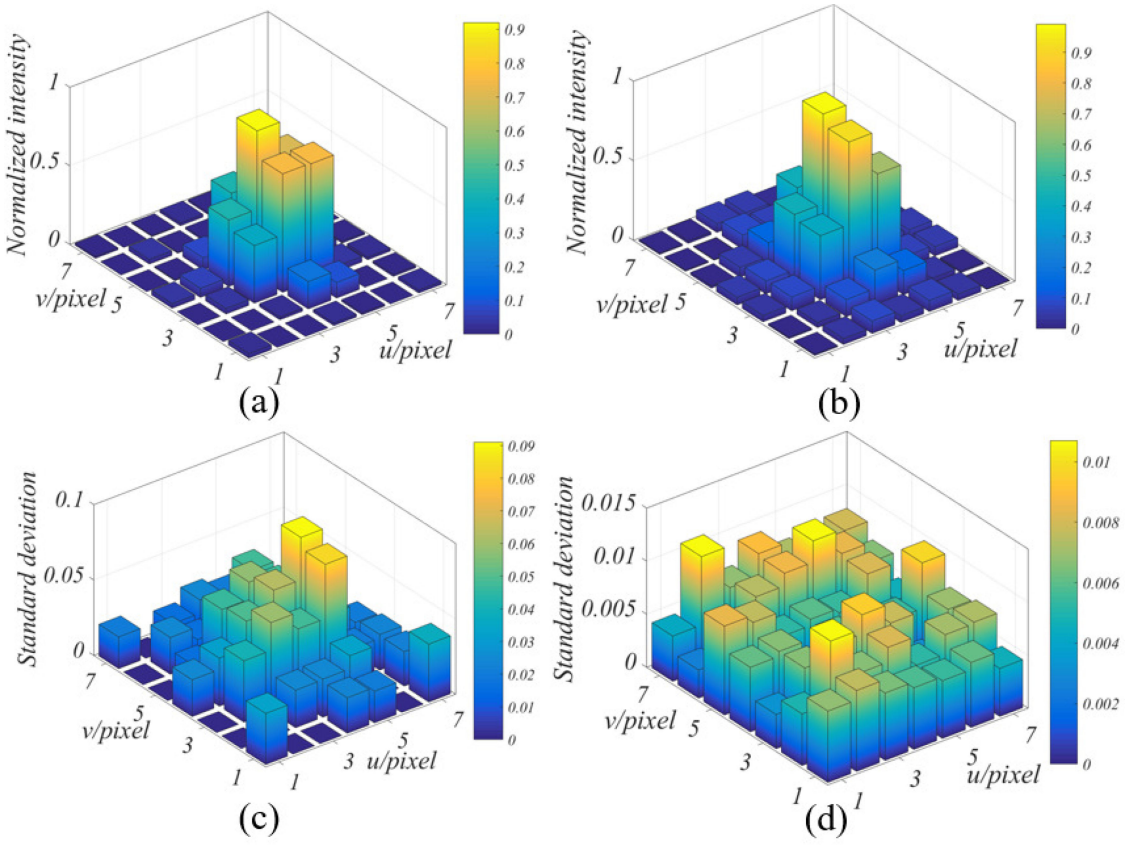


Fig. 10. PSF comparison results between the conventional and proposed methods. (a) Mean PSF results of the conventional method. (b) Mean PSF results of the proposed method. (c) Standard deviation of the PSF result using the conventional method. (d) Standard deviation of the PSF result using the proposed method.

### 3.2 Comparing the PSF Results

The proposed method aims to measure the spatially varying PSF from the perspective of camera pixels. Meanwhile, the SNR of the PSF measurement result is improved by applying SPI to the PSF measurement. In this part of the experiment, we compared the measured PSF result using the proposed method with that using the conventional method. We mainly concentrated on the fluctuation of the result of multiple experiments to determine the noise level of the PSF results because the ground truth of the PSF is unavailable.

We repeated the experiments mentioned in Section 3.1 eight times. The eight results of PSF $h(8, 12; u, v)$ were acquired using the conventional and proposed methods. The value of the PSF was mapped to $[0,1]$. For each experiment, to acquire the spatially varying PSF at every pixel of a $24 \times 24$ area, the number of the required images is $24 \times 24 \times 2$ for proposed method and $24 \times 24$ for conventional method. To ensure the fairness of the comparison, two images were averaged to obtain the PSF result at one pixel for conventional method. Therefore, the number of required images to measure PSF at every pixel is identical for both methods. The mean value of the eight results for both methods are shown in Figs. 10(a) and 10(b). We considered the value of each pixel as an independent variable and calculated the standard deviation of the measured result for each pixel, as shown as follows:

$$\sigma = \sqrt{\frac{1}{N-1} \cdot \sum_{i=1}^{N} (x_i - \bar{x})^2}, \tag{8}$$

TABLE 1
Mean Standard Deviation of the Conventional Method on Different Exposure Time

| Exposure Time T/s | 1/60 | 2/60 | 3/60 | 4/60 | 5/60 | 6/60 | 7/60 | 8/60 |
|---|---|---|---|---|---|---|---|---|
| Standard Deviation/$10^{-5}$ | 2522.3 | 1302.0 | 1072.6 | 1016.2 | 723.2 | 721.8 | 583.2 | 510.5 |

TABLE 2
Mean Standard Deviation of Proposed Method

| Exposure Time T/s | 1/60 |
|---|---|
| Standard Deviation/$10^{-5}$ | 662.8 |

where N denotes the times of measurement, $x_i$ represents the value of one pixel of the PSF in experiment $i$, and $\bar{x}$ is the mean value of $x_i$. The experiment result of the standard deviation for the conventional and proposed methods is shown in Figs. 10(c) and 10(d). To fit the 60 Hz refresh frequency of the LCD screen, the camera exposure time for both methods was preferably set as an integer times of 1/60s.

We find that the mean standard deviation of the proposed method is considerably less than the conventional method by calculating the mean value of the standard deviation images for both methods. We also increased the camera exposure time of the conventional method and acquired the mean value of the standard deviation image. The result is shown in Table 1 and Table 2. The conventional method should increase the exposure time to seven times of the proposed method to achieve a similar mean standard deviation value as the proposed method. Therefore, the result fluctuation of the proposed method is considerably less than the traditional method with the same exposure time. This result indicates that the proposed method can efficiently improve the SNR of the spatially varying PSF measurement.

Furthermore, as mentioned in Section 2, the proposed method can obtain PSF from the perspective of the camera pixels. We conducted an experiment for the quantitative comparison of the PSF result by the proposed method from the perspective of camera pixels with that by the conventional method from the perspective of object points.

We displayed a sharp image with the resolution of 149 $\times$ 90 pixels [Fig. 11(a)] on the LCD screen and used a camera to capture the image. The sharp image was blurred by the camera lens and occupied 90 $\times$ 55 camera pixels [Fig. 11(b)].

Then, we blurred the sharp image using the PSF acquired by the proposed method [Fig. 12]. We applied the proposed method to measure the spatially varying PSF $h(x, y; u, v)$ from the perspective of camera pixels based on FSI. The FSI result of the pixel (u, v) can be regard as a specialized kernel $h(x, y; u, v)$ for the pixel to blur the sharp image. The process of generating the blurred image can be expressed as:

$$g(u, v) = \sum_{x=0}^{M-1} \sum_{y=0}^{N-1} f(x, y) \cdot h(x, y; u, v), \tag{9}$$

where $f$(x, y) is the original sharp image with the resolution of M $\times$ N, $g(u, v)$ is the generated blurred image, $(x, y)$ is the 2D Cartesian coordinates on the LCD plane, $(u, v)$ is the 2D Cartesian coordinates on the camera pixel plane. Thus, the pixel value of the generated blurred image can be directly obtained by calculating the inner product between the specialized kernel and the sharp image. The generated image is shown in Fig. 11(c).

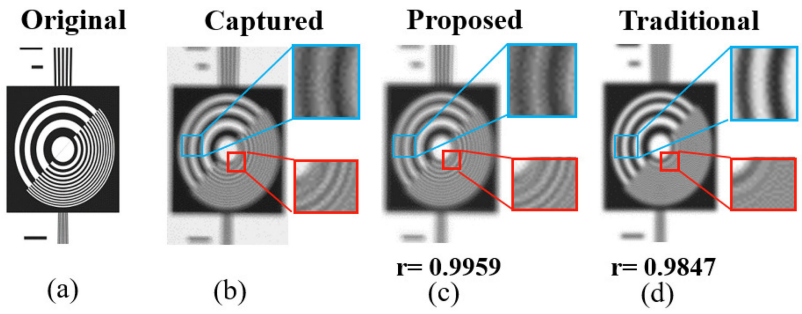


Fig. 11. Comparison of the accuracy of the blur model. (a) Original sharp image displayed on the LCD screen. (b) Image captured by the camera. (c) Generated blurred image using PSF from the perspective of camera pixels measured by the proposed method. (d) Generated blurred image using PSF measured by the traditional method and fitted by the Gaussian model. The image shown in Fig. 11(c) is more similar to the image in Fig. 11 (b) than the image in Fig. 11 (d). The correlation coefficients between the generated images and the images captured by the camera are 0.9959 for proposed method and 0.9847 for the traditional method.

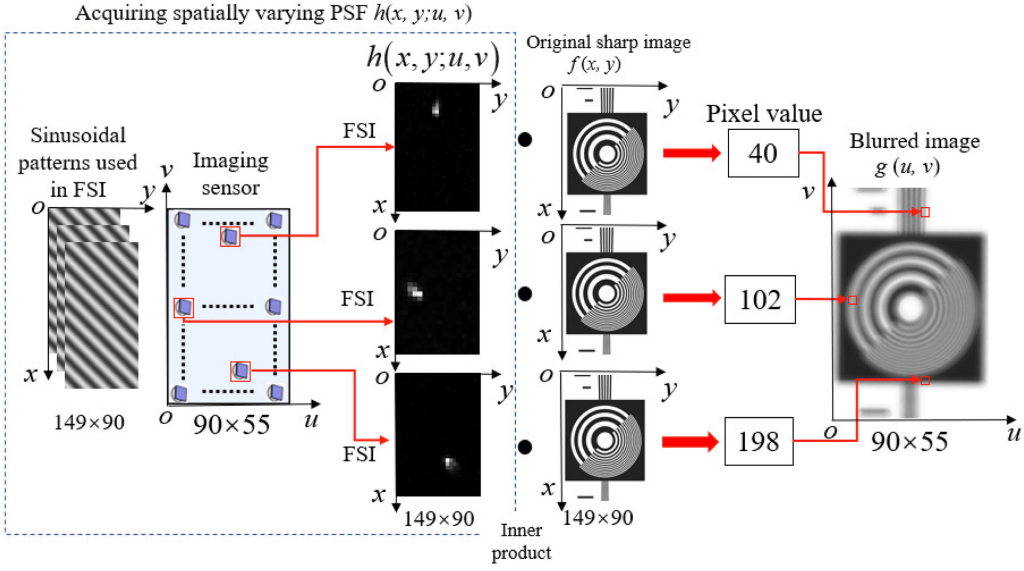


Fig. 12. The schematic diagram of generating the blurred image using PSF obtained by proposed method. Applying FSI to all the pixels, a specialized kernel for each pixel can be acquired. And the pixel value of the blurred image can be obtained by calculating the inner product between the specialized kernel and the sharp image.

Moreover, we displayed a white dot on the screen and obtained a traditional PSF distribution on the camera pixels. A Gaussian model was employed to fit the PSF distribution and convolve the standard image. Then, the standard image was resized to 90 $\times$ 55. The generated blurred image is shown in Fig. 11(d).

Intuitive perception of the images in Fig. 11 shows that the image in the blue box in Fig. 11(d) is sharper than the image in Fig. 11 (b), whereas the image in the red box in Fig. 11(d) is fuzzier than that in Fig. 11(b). However, the image in Fig. 11(c) remains the same in both selected area as the image in Fig. 11(b). Therefore, the proposed method can generate a more accurate blurred image than the traditional method.

We calculated the accuracy of the blurred images using the correlation coefficient r between the generated blurred images and the captured images. The correlation coefficient increases with the

image resemblance and is defined by

$$r = \frac{\sum_m \sum_n \left(A_{mn} - \overline{A}\right) \cdot \left(B_{mn} - \overline{B}\right)}{\sqrt{\left(\sum_m \sum_n \left(A_{mn} - \overline{A}\right)^2\right)\left(\sum_m \sum_n \left(B_{mn} - \overline{B}\right)^2\right)}}, \tag{10}$$

where r denotes the correlation between the two images; A and B represent the image matrix with indexes $m$ and $n$; and $\bar{A}$ and $\bar{B}$ are the mean values of matrixes A and B, respectively.

The correlation coefficients between the images captured by the camera and the generated images are shown in Fig. 11. The correlation coefficient is 0.9959 for the proposed method, whereas 0.9847 for the traditional method. The comparison of the correlation coefficients indicates that the proposed method can provide a more accurate model to fit the camera blur compared with the traditional Gaussian model.

## 4. Conclusion

We use the SPI technology for PSF measurement. The proposed method excels at measuring the spatially varying PSF and achieves high SNR measurement without a laser source. It can also acquire PSF from the perspective of camera pixels, which can provide an accurate model to fit the camera blur.

The key idea of the proposed method is to regard the spatial variant PSF as the light transport coefficients between the object and image points. By employing the SPI technology, the visible region of the scene observed by the camera pixel can be measured by proposed method, which can be regarded as the PSF obtained from the perspective of camera pixel. The SNR of PSF measurement can also be improved by proposed method.

Any type of the SPI method can be adopted to obtain the light transport coefficients. SPI methods based on orthogonal bases, such as FSI, can reconstruct high-quality images. Thus, we adopt the FSI to achieve an accurate PSF measurement.

However, the proposed method has limitations. Using the proposed method to measure the PSF of the entire field of view of the camera is time consuming, and we had to resort to measuring the PSF of multiple small areas in parallel. In our future works, a time-saving method for measuring the PSF through the entire field of view of the camera based on SPI will be investigated.

The proposed method is experimentally capable of measuring accurate spatial variant PSF of the camera lens with high SNR and does not require a laser source. Future research in PSF measurement could benefit from the proposed method when laser source is not applicable. Moreover, the proposed method is adaptive when the spatial variant PSF is required.

## References

[1] T. Lauer, "Deconvolution with a spatially-variant PSF," *Proc. SPIE*, vol. 4847, pp. 167–173, 2002.
[2] L. Sun, S. Cho, J. Wang, and J. Hays, "Edge-based blur kernel estimation using patch priors," in *Proc. IEEE Int. Conf. Comput. Photography*, 2013, pp. 1–8.
[3] T. S. Cho, S. Paris, B. K. Horn, and W. T. Freeman, "Blur kernel estimation using the radon transform," in *Proc. IEEE Conf. Comput. Vis. Pattern Recognit.*, 2011, pp. 241–248.
[4] N. Joshi, R. Szeliski, and D. J. Kriegman, "PSF estimation using sharp edge prediction," in *Proc. IEEE Conf. Comput. Vis. Pattern Recognit.*, 2008, pp. 1–8.
[5] A. Mosleh, P. Green, E. Onzon, I. Begin, and J. M. P. Langlois, "Camera intrinsic blur kernel estimation: A reliable framework," in *Proc. IEEE Conf. Comput. Vis. Pattern Recognit.*, 2015, pp. 4961–4968.
[6] E. Kee, S. Paris, S. Chen, and J. Wang, "Modeling and removing spatially-varying optical blur," in *Proc. IEEE Int. Conf. Comput. Photography*, 2011, pp. 1–8.
[7] J. Brauers, C. Seiler, and T. Aach, "Direct PSF estimation using a random noise target," *Proc. SPIE*, vol. 7537, 2010, Art. no. 75370B.
[8] H. Du and K. J. Voss, "Effects of point-spread function on calibration and radiometric accuracy of CCD camera," *Appl. Opt.*, vol. 43, no. 3, pp. 665–670, 2004.
[9] J. Lehr, J. B. Sibarita, and J. M. Chassery, "Image restoration in X-ray microscopy: PSF determination and biological applications," *IEEE Trans. Image Process.*, vol. 7, no. 2, pp. 258–263, Feb. 1998.

[10] J. Jemec, F. Pernuš, B. Likar, and M. Bürmen, "2D sub-pixel point spread function measurement using a virtual point-like source," *Int. J. Comput. Vis.*, vol. 121, no. 3, pp. 391–402, 2017.
[11] F. A. Navas-Moya, J. L. Nieves, E. M. Valero, and E. Garrote, "Measurement of the optical transfer function using a white-dot pattern presented on a liquid-crystal display," *J. Eur. Opt. Soc.*, vol. 8, 2013, Art. no. 13029.
[12] M. F. Duarte *et al.*, "Single-pixel imaging via compressive sampling," *IEEE Signal Process. Mag.*, vol. 25, no. 2, pp. 83–91, Mar. 2008.
[13] H. Jiang, S. Zhu, H. Zhao, B. Xu, and X. Li, "Adaptive regional single-pixel imaging based on the Fourier slice theorem," *Opt. Exp.*, vol. 25, no. 13, pp. 15118–15130, 2017.
[14] Z. Zhang, X. Ma, and J. Zhong, "Single-pixel imaging by means of Fourier spectrum acquisition," *Nature Commun.*, vol. 6, 2015, Art. no. 6225.
[15] Z. Zhang, X. Wang, G. Zheng, and J. Zhong, "Hadamard single-pixel imaging versus Fourier single-pixel imaging," *Opt. Exp.*, vol. 25, no. 16, pp. 19619–19639, 2017.
[16] L. Bian, J. Suo, X. Hu, F. Chen, and Q. Dai, "Efficient single pixel imaging in Fourier space," *J. Opt.*, vol. 18, 2016, Art. no. 085704.
[17] L. Bian, J. Suo, Q. Dai, and F. Chen, "Experimental comparison of single-pixel imaging algorithms," *J. Opt. Soc. Amer. A*, vol. 35, no. 1, pp. 78–87, 2018.
[18] W. Pratt, J. Kane, and H. C. Andrews, "Hadamard transform image coding," *Proc. IEEE*, vol. 57, no. 1, pp. 58–68, Jan. 1969.